Temporal Analysis of Site-Level Methane Emissions from Nearly One Thousand Upstream Oil and Gas Facilities Equipped with Fixed-Point Continuous Monitoring Systems

David Ball, Nathan Eichenlaub, Ali Lashgari, and Noah Metzger

Project Canary, Denver, CO
Correspondence: david.ball@projectcanary.com

Preprint submitted to EarthArXiv

March 2026

Conflict of Interest Statement

At the time of this study, all authors were employed by Project Canary, which manufactures and operates the continuous monitoring systems used in this study.

Temporal Analysis of Site-Level Methane Emissions from Nearly One Thousand Upstream Oil and Gas Facilities Equipped with Fixed-Point Continuous Monitoring Systems

David Ball[1], Nathan Eichenlaub[1], Ali Lashgari[1], and Noah Metzger[1]

[1]Project Canary, Denver, CO (All authors contributed equally to this work. The author list is ordered alphabetically by surname.)

Correspondence: David Ball (david.ball@projectcanary.com)

Abstract. Temporal variability in methane emissions from oil and gas facilities may significantly impact the accuracy of measurement-based emissions inventories and the effectiveness of measurement-based mitigation policies. Yet the existing knowledge of duration, frequency, and magnitude of emission events remains very limited. A deeper understanding of these temporal characteristics is therefore essential for designing monitoring strategies, interpreting top-down assessments, and prioritizing mitigation actions. This study analyzes methane emissions from 940 upstream oil and gas production facilities equipped with fixed-point continuous monitoring systems (CMS) across seven U.S. basins to investigate site-level emission rate distributions and anomalous emission event durations. Site-level emissions are estimated every 15 minutes using a recursive Bayesian inversion that assimilates in situ methane and meteorological measurements, yielding approximately 24.7 million rate estimates. We employ a facility-specific rolling baseline calculation and apply rate thresholding to identify discrete emission events (emissions that significantly exceed a slowly-varying temporal site-specific baseline), which are then characterized in terms of event-average rate and duration. Across all facilities, approximately 80–90% of estimated methane mass originates from periods when emissions are below 100 kg/hr, indicating that non–super-emitting conditions dominate cumulative mass budgets. The facility-level emissions distribution is highly skewed, with 10.6% of sites responsible for 50% of total inferred mass. Although only 3.7% of emission rate estimates are classified as *event* operational states, these events account for 41% of total emissions, with the majority of event mass arising from intermittent, moderate-rate anomalies.

1 Introduction

Methane is a short-lived potent greenhouse gas (GHG) with a significantly higher global warming potential (GWP) compared to carbon dioxide (estimated to have a 100-year GWP of 27–30 and 20-year GWP of 81–83) (Masson-Delmotte et al. 2021). According to the United States Environmental Protection Agency (USEPA), methane emissions are responsible for approximately 12% of US anthropogenic greenhouse gas emissions, with enteric fermentation associated with domestic livestock, natural gas systems, and decomposition of wastes in landfills being the primary sources (USEPA 2025). Upstream oil and

gas (O&G) production contributes 59% of methane emissions from the oil and natural gas industry (USEPA 2024), making effective management of these emissions critical for mitigating climate change.

Quantifying site-level emissions from O&G facilities is essential for understanding how individual facilities contribute to total emission profiles and for prioritizing mitigation efforts. However, accurate quantification is challenging due to the inherent temporal and spatial variability of methane emissions (Wang et al. 2022; IJzermans et al. 2024; Omara et al. 2024). Intermittent (snapshot) measurement methods have limited capability to capture temporal variability, motivating the deployment of fixed-point continuous monitoring systems (CMS), which can provide time-resolved, facility-specific emission data over extended periods.

Fixed-point CMS have been widely deployed at O&G production facilities over the past several years. Early applications focused on anomaly detection, using algorithms ranging from static concentration thresholds to signal processing and machine learning methods to generate event notifications from raw methane concentration data. More recently, CMS capabilities have expanded to include emission source localization and rate quantification. It is important to distinguish, however, between the raw measurements collected by CMS (methane concentrations at a sparse set of sensor locations) and the derived emission rate estimates that require substantial algorithmic processing. Converting point-sensor concentration and meteorological observations into facility-level emission rates involves atmospheric dispersion modeling, inverse methods, and various assumptions about source geometry and transport conditions. These quantification algorithms remain an area of active research and continued improvement, and their performance under diverse operational and environmental conditions is the subject of ongoing independent evaluation efforts (Bell et al. 2023; Ilonze et al. 2024; Cheptonui et al. 2025; Hossain et al. 2026). These studies have shown year-over-year improvement in the quantification and localization accuracy of some CMS. However, significant uncertainty remains in rate estimates, and performance varies considerably across vendors, reflecting differences in both hardware specifications and the dispersion and inversion methodologies each system employs. With these caveats in mind, validated CMS quantification can provide a semi-continuous, time-resolved view of site-level emissions that characterizes both short-duration and persistent events, bounds their onset and termination in time, and complements other measurement modalities with site-specific meteorological context.

Reconciling emission estimates across measurement technologies and with bottom-up inventories requires explicit treatment of temporal variability. Multiscale measurement campaigns have demonstrated that snapshot measurements at a single facility can vary by over three orders of magnitude due to intra-day and day-to-day variability, limiting their direct applicability to annualized inventory estimates (Wang et al. 2022). Using continuous monitoring data, Wang et al. further characterized distributions of emission event frequency and duration, finding that a large fraction of CMS-detected events lasted less than two hours, many attributable to transient operational activities such as blowdowns. Building on this work, Daniels, Wang, et al. (2023) used CMS data to provide temporal context for snapshot aerial measurements and to construct measurement-informed site-level inventories, demonstrating the essential role of high-frequency data in bridging gaps between top-down measurements and bottom-up estimates. A related challenge for concentration-based event detection is wind-dependent observability: when wind does not carry the plume to a sensor, an ongoing emission produces no enhanced concentrations, potentially causing

duration underestimates. Daniels, Jia, and Hammerling (2024) developed a probabilistic duration model to correct for these nondetect periods, demonstrating that failing to account for them can lead to duration underestimates of up to a factor of 65 on a typical production site. At the basin scale, Barkley et al. (2025) used continuous tower-based methane observations in the Delaware basin to characterize temporal emission patterns, finding that daytime emissions were approximately 27% higher than nighttime, a bias that could affect methodologies relying on daytime-only sampling.

High detection limits present an additional challenge for many aerial and satellite measurements, which generally do not span the full distribution of emission sizes. Although some technologies, particularly aircraft-based LiDAR systems, have achieved detection thresholds on the order of a few kg/hr, most satellite and aerial platforms operate at substantially higher limits, and even sensitive technologies may not detect all emitting sources during a single overflight. A recent study estimates that in 2021, 70% of upstream and midstream O&G methane emissions nationally originated from facilities emitting less than 100 kg/hr, with facilities below 10 kg/hr contributing approximately 30% of total emissions (Williams et al. 2025). This fraction varies by facility type, with upstream production sites contributing a larger share of emissions from sub-100 kg/hr facilities compared to midstream infrastructure. The pattern holds across top-producing basins, where 60–86% of methane emissions originate from facilities emitting less than 100 kg/hr. The accuracy of top-down inventories therefore depends heavily on how emissions below detection limits are treated, including both sub-threshold sources within detected facilities and entire facilities operating below detection (Williams et al. 2025). Despite the substantial collective contribution of these lower-emitting facilities, their temporal emission characteristics remain poorly understood, representing a significant research gap.

This study analyzes continuous methane measurement data from 940 upstream O&G production facilities equipped with fixed-point CMS across multiple U.S. production basins to investigate site-level emission rate distributions and the characteristics of anomalous emission events. While emission distributions vary across basins and individual facilities, this dataset provides a broad view of how facilities with relatively lower emission rates contribute to overall sectoral emissions. The findings are intended to complement other measurement modalities by providing temporally resolved context for site-level and basin-wide emission estimates and to inform the design of measurement and mitigation strategies.

2 Data and Methods

2.1 Data

This study uses continuous methane emission measurement data collected using fixed-point CMS from 940 upstream oil and gas facilities across seven basins, with approximately 88% of the wellpads located in Haynesville and Appalachian basins. The typical equipment present on these facilities includes wellheads, gas processing units (GPUs), separators, and tanks, with an average facility area of 3,936 square meters. The data used for this analysis spans from May of 2024 through May of 2025.

The data in this study were gathered using a CMS solution that utilizes tunable diode laser spectroscopy (TDLAS). These sensors are housed within a cloud-connected integrated device (the Canary X), that can also be equipped with a 2D ultrasonic

anemometer, which is essential for quantifying emissions from point-sensor data. The TDLAS methane sensors used in this study offer 0.4 ppm sensitivity, $\pm 2\%$ accuracy, and a precision of $\leq$0.125 ppm with 60-second averaging. While the device samples at 1 Hz, the data are typically aggregated into 1-minute averages for analysis and quantification.

A typical CMS configuration includes 3 to 4 nodes of fixed-point sensors along with one 2D sonic anemometer per facility. The CMS sensors are placed within the facility boundaries. For meteorological data, the 2D ultrasonic anemometers acquire wind measurements (wind speed and direction) at 1 Hz frequency, which are subsequently aggregated into 1-minute averages for use in the analysis. These instruments are calibrated following standard guidelines (Bailey 2000) to ensure accurate data. Data collected during very low wind speeds (< 0.5 m/s) are excluded, as these conditions produce complex plume dynamics that are difficult to model reliably.

2.2 Methodology

In order to estimate a facility's emission rate every 15 minutes from a sparse network of stationary point sensors, potential emission points are manually labeled and a forward dispersion model is used to simulate the transport of gas from every potential source to every sensor on the facility, accounting for wind speed, direction, atmospheric stability, as well as source/sensor locations and heights. A recursive Bayesian estimator is then applied to assimilate concentration and in-situ meteorological measurements, minimizing the difference between simulated and measured concentrations under certain constraints and regularization, while taking into account the previous estimate of the source rates and associated uncertainties. Notably, this approach is inherently robust to wind-dependent observability gaps: once elevated emission rates are assigned to sources, these rates are not reduced until both the sensor measurements decrease and the wind direction is favorable for transport from source to sensor. This behavior addresses the same wind-dependent observability concern raised by Daniels, Jia, and Hammerling (2024), in that emission estimates persist through periods of unfavorable wind rather than being artificially truncated by non-detect intervals. We refer to previous works for a more detailed description of quantification methodologies, encompassing different forward dispersion models and inverse frameworks (Ball, Eichenlaub, and Lashgari 2025; Ball, Ismail, et al. 2025; Daniels, Nychka, and Hammerling 2025), and to Cheptonui et al. (2025) for the most recent third-party-administered blind testing results.

2.2.1 Emission Rates

This work analyzes approximately 24.7 million 15-minute site-level emission rate estimates across 940 production well sites. The site-level emission rates encompass vented, combusted, and fugitive categories, where vented and combusted emissions represent expected operational releases, while fugitive emissions are unintentional leaks. No attempt was made to filter out operational emissions due to the absence of the necessary operational activity data.

Sections 2.2.2 and 2.2.3 describe how a continuous quantification estimate is segmented into discrete emission events in an attempt to capture relatively high-rate anomalous emissions that significantly exceed a temporally varying site-specific baseline. It is worth noting that several subjective choices have to be made in this process, from the baseline estimation (length

of the smoothing window and relevant statistics to consider) to the event detection (thresholding and merging criteria). The following sections provide justifications and explanations for these choices, but are not to be interpreted as globally-applicable processes for baseline estimation and event detection: there may be circumstances in which this particular set of choices does not adequately capture the intended behavior (e.g., large midstream sites that have very high baselines that vary with the number of active compressors).

2.2.2 Site-Specific Baseline Emissions

For each facility, a site-specific baseline is computed as the 3-day rolling average of the 25th percentile of the mass emission estimate from a given facility. This approach is intended to represent background emissions under normal operating conditions, while the rolling window allows the baseline to adapt gradually to fluctuations in operational emissions, e.g., during periods of particularly high throughput, pneumatic actuation, etc. The 3-day window length provides a balance between responsiveness to sustained changes in operations and temporal smoothing to avoid overreacting to day-to-day variability or noise inherent in the emissions estimates. An upper bound of 5 kg/hr is imposed on this baseline, ensuring that high-rate long-duration events are not erroneously considered part of the baseline. We note that this choice is only justifiable because of the particular types of sites in this dataset: these are all relatively simple upstream production sites (sites with compressors have been filtered out), and as such, standard operating emissions (excluding maintenance, blowdowns, etc.) are expected to be relatively small. This ceiling affects 1.4% (428,685) of the baseline data points.

2.2.3 Operational States and Designation of Emission Events

We classify each facility's operational status into two distinct states: normal operations, where facilities emit at their typical baseline levels, and emission events, which represent periods when emissions substantially exceed these baseline levels, potentially due to equipment malfunctions, operational upsets, or other anomalous conditions. Without additional operational data, it is impossible to distinguish between expected and fugitive emissions. As such, we make no attempt to do so in this study. The "event state" refers only to whether the estimated emissions are *unusually* high, relative to an understanding of the baseline emissions from a given facility.

To identify emission events, we subtract the baseline emission rate from the emission estimate; this signal quantifies how much current emissions exceed normal operating conditions. An event begins when the signal exceeds 5 kg/hr i.e., when measured emissions rise more than 5 kg/hr above baseline. Once initiated, the event continues until the signal drops below 2.5 kg/hr, indicating that emissions have returned to a value that is consistent with the baseline. This asymmetric threshold approach, with a higher threshold for event initiation than termination, introduces hysteresis that prevents rapid switching between event and "non-event" states when emissions fluctuate near the detection threshold. This provides more stable event characterization that avoids breaking up one long emission event into several events due to inherent noise in the quantification estimation.

During long-duration high-rate emission events, the rolling baseline calculation could become artificially inflated if these elevated emissions were incorporated into the baseline statistics. To preserve the integrity of the baseline, we implement a "freeze"

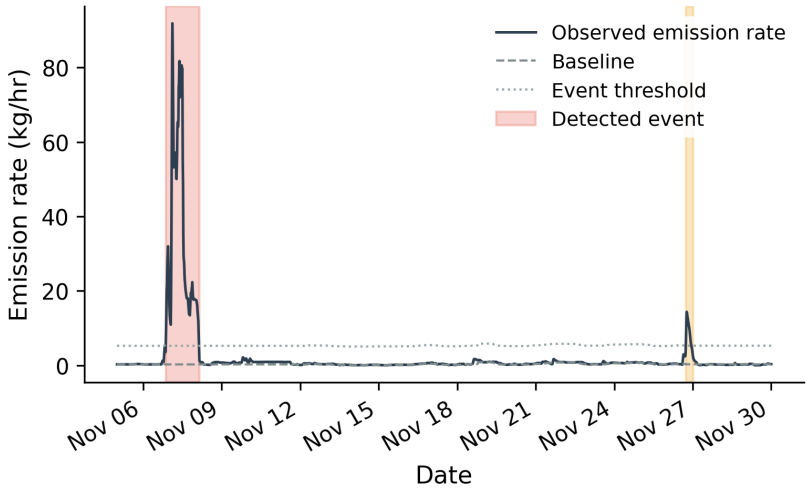

Event	Duration (hrs)	Mean (kg/hr)	Peak (kg/hr)
1	31	34.9	91.9
2	6	8.6	14.4

Figure 1. Example of quantification estimate (black), estimated baseline (dashed gray), event threshold (dotted gray), and distinct detected emission events (shaded regions) from a randomly selected facility and period of time. The characteristics of these emission events are shown in the table (right).

procedure: when an event is detected, we calculate the 24-hour average baseline immediately preceding the event start and hold this value constant throughout the event duration and for three days following event termination. This approach ensures that the baseline remains representative of true normal operations, prevents elevated emissions from contaminating future baseline calculations, and avoids masking subsequent events with an artificially inflated baseline. After the three-day post-event period, the baseline resumes its normal rolling calculation, allowing it to adapt to genuine changes in facility operations while remaining robust against transient emission spikes.

Finally, we apply a post-processing step to merge events that occur within two hours of each other into single continuous episodes. This merging addresses two practical considerations: first, the inherent noise in quantification estimates can cause the signal to briefly dip below the termination threshold before rising again, creating artificial fragmentation; and second, a single operational issue may generate multiple emission pulses in close succession that are more reasonably treated as one extended event. By consolidating these closely-spaced emissions, we reduce over-fragmentation and limit the influence of measurement noise on event statistics. Through this approach, we transform continuous emission measurements into discrete, interpretable events that can be analyzed in terms of durations and rates for the purposes of gaining insight into the statistics of these distributions.

To illustrate this process of event detection from the continuous quantification estimate, we show in Figure 1 a randomly selected site's quantification curve and associated emission events over a random time period. Here, the black curve shows the quantification estimate, the dashed gray line depicts the baseline (the 3-day rolling 25th percentile in quantified rate), the dotted

gray line shows the threshold that must be crossed to trigger an event detection, and the shaded regions indicate emission event detections.

3 Results

In Section 3.1, we analyze the relative contribution to the total estimated emissions from rates of varying magnitudes, without making distinctions between "event" and "non-event" states, and examine how these insights relate to previous measurement campaigns. Additionally, we examine the relative contribution to the total emissions by site. Next, in Section 3.2 we break out the total mass and temporal duration between event and non-event operational statuses and further compare these distributions broken down between the high-emitting and low-emitting sites identified in Section 3.1. Finally, in Section 3.3, we analyze the joint distribution of emission event rate and duration and provide insights into the relative contribution to the total mass from different combinations of event duration and rate, highlighting the importance of intermittent emitters.

3.1 Distribution of Site-Level Emission Rate

In this section, we analyze the 24.7 million individual emission rate estimates and their contributions to the cumulative estimated mass over the full dataset. In order to illustrate the sampling uncertainty, we bootstrap 500 iterations of a small sample (0.1%) of rate estimates and compute the cumulative mass distribution across each realization to generate an ensemble of cumulative distributions.

To compare our results to previous studies, we overlay the cumulative emissions distribution from recently published facility-level emissions estimates by the EDF (Williams et al. 2025), using the ensemble of cumulative distributions for well sites provided by the authors, in Figure 2. Both the CMS and EDF distributions are shown with median curves and 5th–95th percentile confidence bands. The EDF curve shown here represents all well sites nationally, without distinguishing between low- and high-production facilities. As shown in Williams et al. (2025), when this distinction is made, high-production sites exhibit larger characteristic emission rates, shifting the cumulative emissions curves to the right.

In our CMS-based estimates, approximately 80%–90% of total inferred emissions originate from facilities emitting less than 100 kg/hr (the nominal "super-emitter" threshold). Williams et al. (2025) report that nationally, approximately 70% of upstream and midstream emissions originate from facilities below this threshold, with the fraction varying by production level—approximately 74% for high-production sites and 98% for low-production sites. The CMS-derived distribution is slightly more dominated by higher-rate emissions than the national all-site EDF distribution, which is expected: the sites in our study are all relatively high-producing and do not include marginal wells, whereas the EDF curve reflects a mixture of production levels. A more direct comparison against the EDF high-production sites alone indicates that the CMS distribution is shifted toward lower rates, with a larger fraction of mass originating from sub-100 kg/hr emissions than the 70–78% reported by the EDF for non-marginal well sites. Several factors likely contribute to this apparent discrepancy.

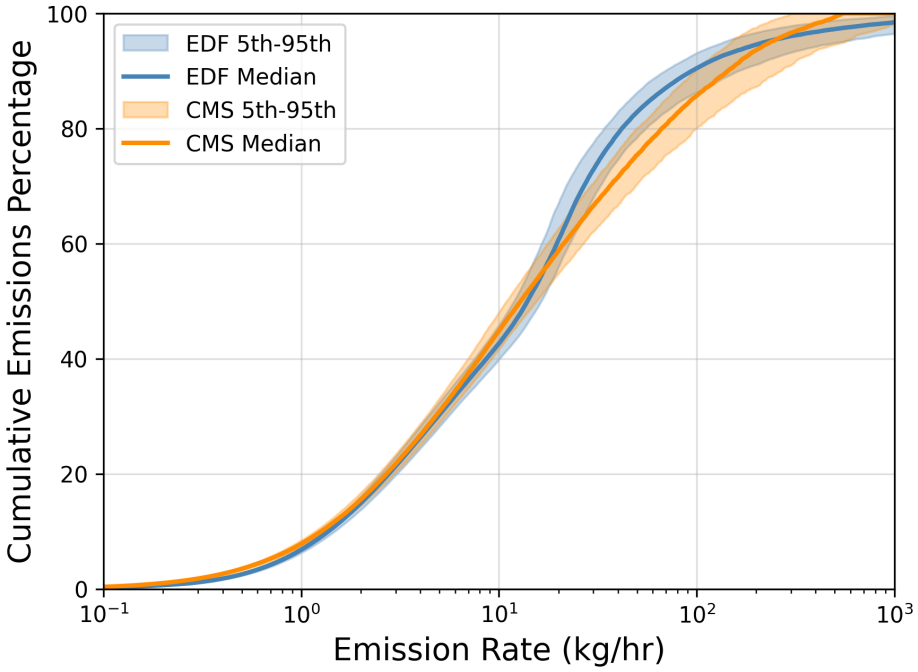

Figure 2. Cumulative percent of total methane emission mass as a function of the emission rate. The orange band and line show the CMS-derived median and 5th–95th percentile bootstrap confidence interval. The blue band and line show the median and 5th–95th percentile from the EDF facility-level emissions estimates (Williams et al. 2025). The EDF curve represents all national well sites without distinguishing between production levels.

First, our analysis focuses on a distinct subset of facilities: it exclusively includes sites equipped with continuous monitoring systems that generate anomalous emission alerts. Facilities with real-time alerting may experience shorter event durations and faster repair times compared to unmonitored sites, which would shift the observed emission distribution toward lower rates. This potential selection effect should be considered when comparing our results to basin-wide surveys of unconditioned facility populations.

Second, the geographic and basin-level composition of our sample differs from prior work. The facilities under this study are concentrated primarily in the Appalachian and Haynesville basins. Previous studies suggest that other basins are often associated with larger emission events compared to the Appalachian and Haynesville basins (Williams et al. 2025; Sherwin et al. 2022). Differences in basin-level infrastructure, operational practices, and other factors may drive systematic shifts in the cumulative emissions curve.

Finally, CMS-based quantification may underestimate some short-duration, high-rate emission events under certain conditions. When the wind direction is such that the plume does not advect directly from the source to one or more sensors, fixed-point sensors may only partially observe, or entirely miss, emission anomalies. The relative impact of such occurrences can be more

pronounced for short-duration events, because any missed portion represents a larger fraction of the event's total duration and mass compared to longer events. The effective source strength can be further mischaracterized if the forward model does not fully account for thermal or chemical buoyancy, pressurized releases, or other dynamics that elevate the plume above the sensor network. These processes are difficult to represent self-consistently with the limited state information typically available from fixed-point CMS. As a result, they can lead to a systematic low bias in estimated rates for a subset of large events.

Despite these differences, the general takeaway is consistent across both the CMS and EDF estimates: emissions from non–super-emitting facilities have an outsized impact on total emissions. Consequently, mitigation strategies that focus exclusively on super-emitters are likely to overlook a large portion of total emissions, underscoring the importance of complementary efforts targeting moderate-rate sources.

In addition to analyzing all emission estimates in aggregate, we partition the data by facility and quantify each site's relative contribution to the total emitted mass over the study period. This facility-level view is important because it reveals how balanced the emission profile is across the asset base, which in turn informs the potential effectiveness of targeted mitigation strategies. If a small number of sites account for a large fraction of total emissions, substantial reductions may be achievable by focusing interventions on a limited set of facilities. Conversely, if emissions are relatively uniform across sites, identifying the most impactful mitigation opportunities becomes more challenging.

Figure 3 shows the cumulative fraction of total emissions as a function of the fraction of sites, after sorting facilities in descending order by total emitted mass. The red line denotes the empirical cumulative emissions curve, and the dashed black line represents a hypothetical perfectly even distribution in which all sites emit the same total mass. The red shaded area between these curves reflects the degree of imbalance in the emission rate distribution across facilities. To quantify this imbalance, we compute the Gini coefficient, which is directly proportional to the shaded area. A value of 1 corresponds to a maximally imbalanced distribution (all emissions from a single site), whereas a value of 0 indicates a perfectly uniform distribution. For our dataset, the Gini coefficient is 0.619, indicating a strongly skewed emissions distribution.

To provide a more intuitive interpretation, we annotate Figure 3 with markers and labels indicating the fraction of sites responsible for 50%, 75%, and 90% of total emissions. Consistent with prior work on facility-level methane emissions distributions (Williams et al. 2025), we find that a relatively small subset of sites—99 out of the 940 facilities analyzed—accounts for 50% of the total estimated mass of emissions. For the remainder of this study, we refer to these 99 facilities as "high-emitting" sites and use this classification to stratify subsequent analyses, contrasting the characteristics of high- and low-emitting facilities.

While the specific numerical values may differ from those reported in other studies due to differences in basins, operational practices, and measurement approaches, the overarching conclusion is similar: the strongly imbalanced distribution of emissions across sites implies the existence of highly efficient mitigation opportunities concentrated in a relatively small subset of facilities.

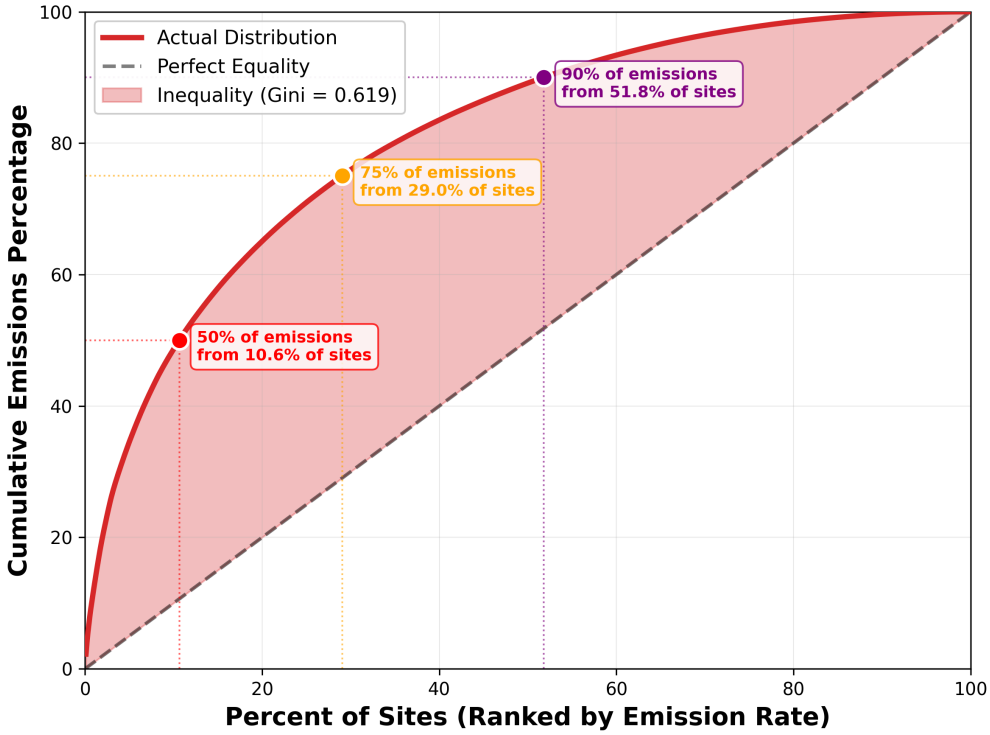

Figure 3. Percentage of total emissions as a function of the percentage of sites, with sites sorted in decreasing order of total mass emitted.

3.2 Emissions During Event vs Non-Event Operational States

In this section, we partition the total cumulative methane emissions into two distinct operational states: (i) slowly varying, relatively small *non-event* operational state, and (ii) temporally distinct periods of elevated emissions, *events*, identified by the event-detection framework described in Section 2.2.3. This breakdown enables us to quantify the relative contributions of near-baseline, *non-event* emissions versus elevated-emission episodes caused by an *event* to the overall mass budget. These two populations are associated with different root causes and mitigation levers, such as routine operational emissions and small releases in the non-event state versus anomalous emissions caused by abnormal process conditions, equipment malfunctions, or maintenance activities. Distinguishing their relative importance is critical for interpreting site-level emissions, reconciling snapshot measurements with continuous data, and prioritizing mitigation strategies.

Figure 4 summarizes the partitioning of both time and mass between *non-event* and *event* operating states for all sites (left), high-emitting sites (middle), and low-emitting sites (right). Site categories follow Section 3.1, where high-emitters are defined as the 10.6% of facilities responsible for 50% of total estimated emissions, and the remaining sites are classified as low-emitters. In the figure, blue bars denote quantities associated with non-event emissions while orange represents quantities associated with

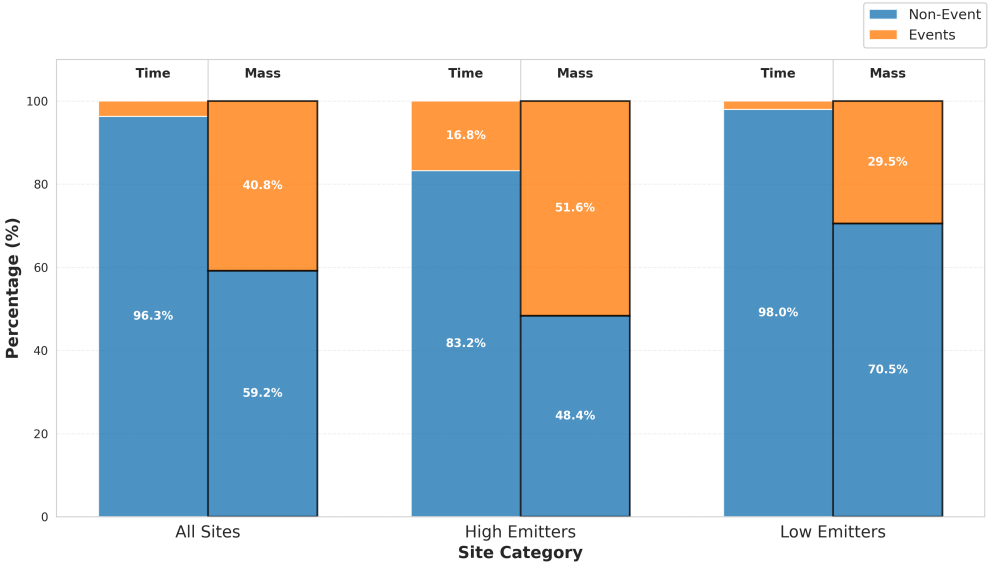

Figure 4. Breakdown of temporal duration and total mass between *non-event* and *event* operational states for all sites (left), high-emitting sites (middle), and low-emitting sites (right)

event emissions. Across all sites (left), we find that only 3.7% of the 15-minute emission rate estimates are labeled as being in an *event* state. Despite their rarity, *event* periods account for 40.8% of the total estimated emissions.

Comparing *event* operational state frequency across site categories, we find that 16.8% of the time associated with high-emitting facilities is classified as an *event* state, versus only 2% for low-emitting sites—an approximately eightfold increase in *event* occurrence. A similar pattern emerges in the total estimated emissions mass: for low-emitting sites, 29.5% of total emissions are associated with *event* operational state, whereas for high-emitting sites, 51.6% of total emissions occur during *event* periods.

3.3 Event-level statistics

In Section 3.1, we examined total emissions without distinguishing whether a site was operating at a typical *non-event* state or in an elevated emission *event* occurrence. We now focus specifically on the joint distribution of event duration and emission rate, and on how different classes of events (i.e., different combinations of event duration and magnitude) contribute to the total estimated mass across all events. In this analysis, we first compute the total mass emitted during periods classified as an *event* and use this quantity as the denominator when evaluating the fractional contribution of events with different characteristics (duration, rate) to the total mass budget.

Figure 5 summarizes these patterns in a two-dimensional rate–duration space. Panel A (top left) presents a heatmap of the fractional contribution to total event mass, with the horizontal axis denoting binned mean event rate and the vertical axis

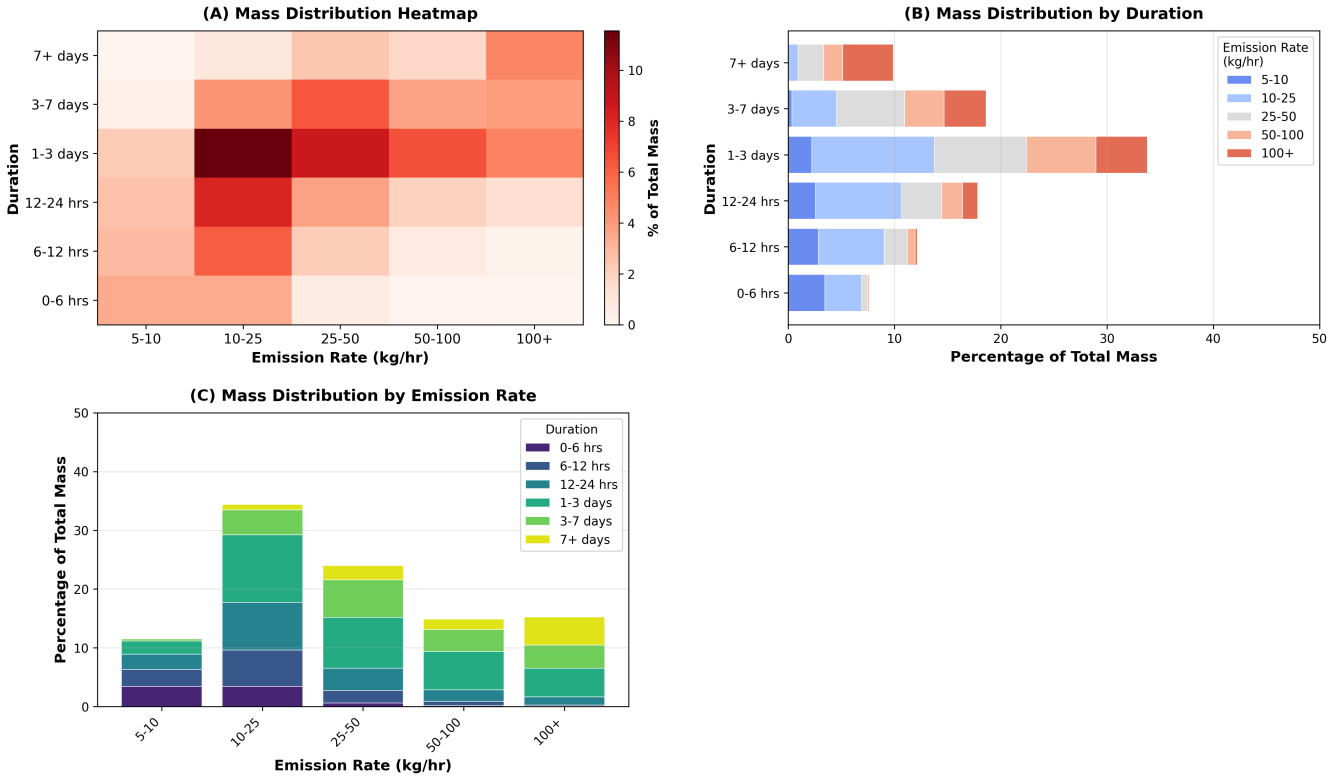

Figure 5. Distribution of methane emissions by event duration and emission rate. (A) Heatmap showing the percentage of total methane mass contributed by events in each duration and emission rate bin. (B) Marginal distribution by duration, showing how emissions within each duration category are partitioned across different emission rates. (C) Marginal distribution by emission rate, showing how emissions within each rate category are partitioned across different durations. Color intensity in panel A represents the percentage of total mass, while stacked bars in panels B and C sum to 100% within each category, illustrating the relative importance of different event characteristics to total methane emissions.

denoting event duration. The color in each cell represents the share of total event mass (in percent) attributable to events whose mean rates and durations fall within the corresponding bin. The adjacent panels (B and C) show the marginal distributions along rate and duration, respectively, obtained by summing the heatmap values along one axis.

The single most influential bin consists of events lasting between 1 and 3 days with mean rates of 10–25 kg/hr, which contributes more to total event mass than any other rate–duration combination. When marginalizing over rate, we find that 33% of total event mass is released by events with durations of 1–3 days, and an additional 37% from events lasting less than 24 hours. In other words, approximately 70% of all mass emitted during identified events is associated with episodes shorter than three days. In contrast, longer-lived events contribute a smaller fraction of the total mass, despite their extended duration, because they tend to occur less frequently.

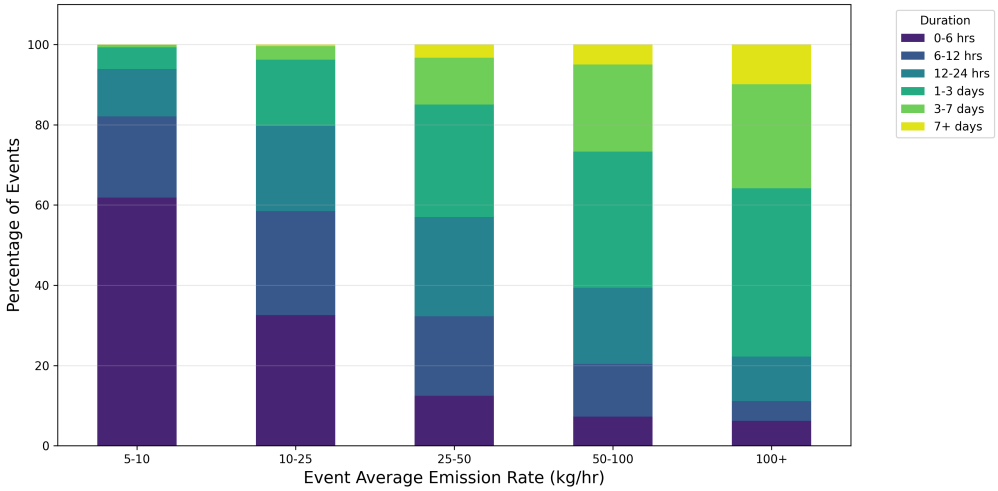

Figure 6. Event duration distribution by emission rate. Percentage breakdown of event durations (stacked bars) across emission rate categories. Numbers above bars indicate total event counts in each emission rate bin. The shift toward longer durations (warmer colors) at higher emission rates indicates that more intense emissions tend to persist longer.

Taken together, these results indicate that the discrete emission events resolved from the high-temporal-frequency CMS record are dominated, in aggregate, by intermittent rather than persistently elevated emissions that last for long periods. This has direct implications for mitigation and detection strategies: a low frequency of measurement using snapshot approaches may misrepresent total site emissions as a substantial portion of the event-associated mass may go undetected, whereas strategies that can reliably detect and resolve short- to intermediate-duration anomalies (on the order of hours to a few days) are likely to capture a large fraction of the emissions attributable to events.

To further clarify how event duration varies across a range of emission rates, and to highlight the intermittent nature of emissions, we present in Figure 6 the frequency of events (not mass-weighted) of a given duration broken out by emission rate. In this representation, each column corresponds to a specific mean emission rate bin and is normalized to sum to unity (i.e., 100%), such that the stacked bars show the relative frequency of different event-duration classes within that rate range.

At low rates (5-10 kg/hr), we find that many events are short-lived: the 0–6 hour duration bin is the most common, indicating that a large fraction of low-rate events are brief. This behavior is consistent with routine, low-emitting operational activities (e.g., pneumatic actuations or short releases) that are inherently transient. In contrast, higher-rate events tend to exhibit longer durations. The majority of events with mean rates exceeding 100 kg/hr persist for 1–7 days, suggesting that large releases are often associated with sustained operational anomalies or delayed repair times. However, even these temporally infrequent, high-rate events are rarely truly persistent: only about 10% of events above 100 kg/hr last longer than 7 days. Overall, the normalized duration–rate distribution underscores that, across a wide range of emission rates, the event population is dominated by short- to intermediate-duration episodes rather than long-lasting elevated emissions.

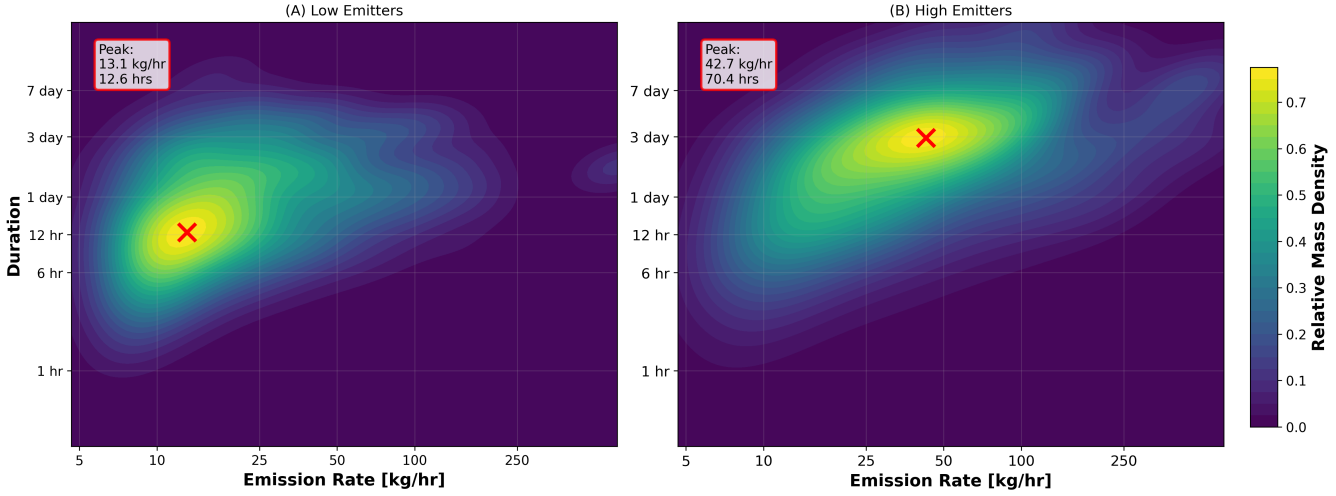

Figure 7. Mass-weighted 2D kernel density distributions of emission rate versus event duration for low emitters (A, bottom 50% by mass) and high emitters (B, top 50% by mass). Red X markers denote distribution peaks.

3.3.1 Event Statistics High-vs-low Emitting Facilities

To explain characteristic differences in emission events between high- and low-emitting facilities, we partition the 940 sites into two groups: "high emitters," the 99 facilities responsible for 50% of total emissions in our sample, and "low emitters," the remaining 841 sites. Because this classification is based on total emitted mass, differences in event characteristics between the two groups are expected; the question is which characteristics (event rate, duration, or frequency) most strongly differentiate them. Specifically, we ask whether enhanced emissions are dominated by long-duration, moderate-rate leaks, by short-duration but very high-rate events, or by some combination of both.

To address this, we construct kernel density estimates (KDEs) in the two-dimensional rate–duration space, separately for high- and low-emitting sites. The resulting distributions are shown in Figure 7, where the background color gradient represents the relative mass density of events for each rate–duration combination. The maxima of the 2D KDEs are indicated by red x's, and the corresponding rate and duration at these peaks are reported in the inset text.

We find that the event distribution for high-emitting sites is shifted toward both longer durations and higher rates compared to low-emitting sites. The peak in relative mass density for high emitters occurs at a mean emission rate of approximately 43 kg/hr and a duration of about 70 hours, whereas for low-emitting sites the characteristic peak occurs at a rate of roughly 13 kg/hr and a duration of only 12.6 hours. In other words, the typical mass-dominant events at high-emitting facilities are about three times larger in rate and roughly six times longer in duration than those at low-emitting facilities, indicating that both event magnitude and persistence contribute to the elevated emissions from this subset of sites.

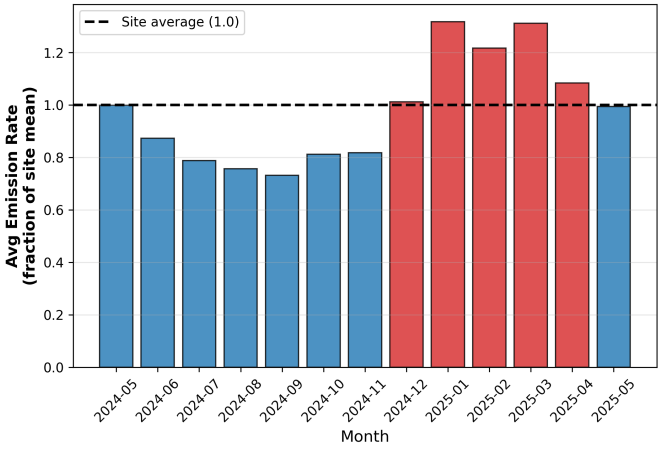

Figure 8. Monthly average of site-normalized emission rates. Each site's 15-minute emission estimates are divided by that site's time-averaged mean, placing all facilities on a common scale where 1.0 represents typical emissions. Values above 1.0 indicate that sites, on average, emitted above their typical levels during that month and are highlighted in red.

4 Seasonality

To investigate potential seasonal patterns in methane emissions, we analyzed the temporal distribution of emission rates across the 13-month observation period (May 2024 through May 2025). We note, however, that this observation period is limited to only a single year, so any patterns observed should be interpreted cautiously and not generalized to other years. For example, this could have been a particularly severe (or mild) winter/summer, which may give rise to different emission characteristics than more typical conditions.

A naive comparison of monthly mean emission rates will be affected by the skewed distribution of site-level emission rates, with a small number of high-emitting facilities contributing disproportionately to total mass (as demonstrated in Section 3.1). In order to address this and more directly assess the seasonal variations across all sites, we compute the time-averaged mean emission rate across all observations for each facility and express each individual 15-minute emission estimate as a fraction of its site's mean, yielding a dimensionless normalized rate. By normalizing within each site before aggregating across facilities, we ensure that a single high-emitting site does not dominate the seasonal signal, allowing each facility to contribute equally to the analysis of seasonal trends.

Figure 8 presents the monthly average of these normalized emission rates across all sites. A clear seasonal pattern emerges: winter and spring months (December 2024 through April 2025) exhibit normalized emission rates above 1.0, while the remainder of the months fall below the average. Our findings are consistent with recent satellite and aircraft based studies that have independently identified seasonal variability in oil and gas methane emissions. Varon et al. (2026) analyzed TROPOMI satellite observations of the Permian Basin from 2019–2023 and found that emissions were on average 50±10% higher in

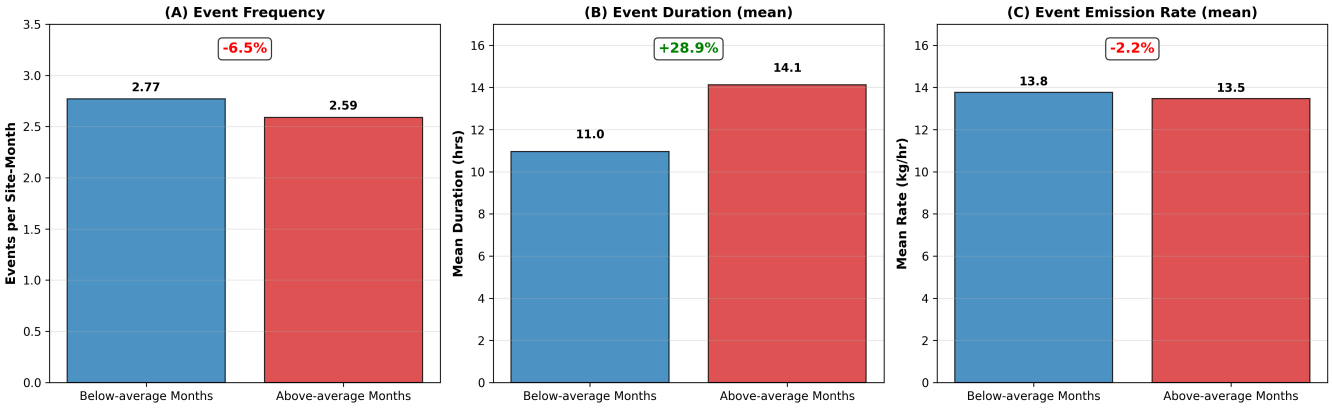

Figure 9. Event frequency (left), average duration (middle), and average emission rate (right) partitioned by above-average and below-average emitting months.

winter (December–February) than in summer (June–August). Similarly, Hu et al. (2025) used inverse modeling of ground and airborne measurements across the continental United States from 2008–2021 and reported that oil and gas sector emissions were approximately 40% higher in winter than summer. We see a similar magnitude of increased emissions between these specific months: the average of the normalized monthly rates for winter months is 1.18, while the average for the summer months is 0.80; the winter months have normalized emission rates that are 46% higher than the summer months, a seasonal fluctuation that is consistent in magnitude with these previous studies.

To identify which factors drive the elevated winter rates, we explore the characteristics of emission events partitioned by whether they fall into "above-average" months (normalized rate >1) or "below-average" months (normalized rate <1). To this end, we compute the event frequency (i.e., the number of emission events per site-month), the average event duration, and the average emission rate of events broken down between the above- and below-average months. These results are shown in Figure 9.

Interestingly, neither the event occurrence rate (expressed in events per site-month) nor the mean event emission rate is higher during above-average months compared to below-average months; the increase in total emissions cannot be attributed solely to more frequent or more severe events. The mean event duration, however (middle panel), shows a significant increase (a near 30% increase in mean event duration) during above-average months. To hone in on this further, we compute the event frequency **only** of events that last more than 48 hours and find that these longer-duration events are 44% more frequent during the above-average months. In other words, from the data available to us at this particular set of sites, we see an increase in emissions during winter and early spring months that is driven by a population of emission events with durations of multiple days that are less common during below-average months.

Interpreting this finding is challenging without additional operational information. It could be that LDAR teams face delays in scheduling repairs during months with more adverse weather conditions, that severe weather conditions result in more fugitive emissions that tend to be longer-lived (on the order of days) compared to operational events (on the order of minutes to hours), or another reason entirely. Understanding the root causes of this seasonal pattern in event duration represents an important direction for future work.

5 Conclusions and Discussions

This study analyzed 24.7 million continuous methane emission rate estimates from 940 upstream oil and gas production facilities equipped with fixed-point continuous monitoring systems (CMS) across seven U.S. basins. Emission rates were estimated at 15-minute intervals using a recursive Bayesian inversion, and the resulting time series were analyzed to characterize the temporal dynamics of site-level methane emissions.

Across all facilities, we find that 80–90% of estimated methane mass is emitted when site-level emission rates are below 100 kg/hr, indicating that non–super-emitting conditions dominate cumulative emissions despite the presence of large events. The distribution of facility-level emissions is highly skewed (Gini coefficient 0.619), with 10.6% of sites (99 out of 940) responsible for 50% of total estimated mass. This imbalance implies that (i) mitigation strategies focused on a relatively small subset of high-emitting facilities can, in principle, deliver disproportionate reductions, and (ii) accounting for the aggregate contribution of numerous lower-emitting sites is critical for accurate sectoral emissions inventories.

Emission events are temporally infrequent but disproportionately impactful. Only 3.7% of 15-minute rate estimates fall in an *event* state, yet these periods account for 41% of total inferred emissions. The mass emitted during these events is dominated by anomalies of moderate rate and limited duration: approximately 70% of total event mass originates from events shorter than three days, with the single largest contribution from events with mean rates of 10–25 kg/hr lasting 1–3 days. Both the frequency and severity of events differ markedly between high- and low-emitting facilities. At high emitters, 16.8% of operating time is classified as an *event* state and 51.6% of mass is emitted during events, compared to 2.0% and 29.5%, respectively, for low emitters. The peak of the mass-weighted event distribution at high emitters (43 kg/hr, 70 hours) is about three times larger in rate and six times longer in duration than at low emitters (13 kg/hr, 12 hours), indicating that elevated emissions at high-emitting facilities arise from events that are both more intense and more persistent.

These results have several implications for measurement-informed inventories and mitigation strategies. First, the dominance of short- to intermediate-duration anomalies in the event mass budget suggests that snapshot campaigns with low revisit frequency are likely to miss a substantial portion of event mass. Moreover, even when snapshot methods do capture an event, temporal extrapolation without site-specific information on emission variability introduces significant uncertainty. More broadly, the temporal characteristics observed here suggest that measurement strategies capable of resolving sub-daily to multi-day anomalies would capture a substantially larger fraction of event-associated emissions than approaches relying on infrequent sampling alone.

Second, the strong facility-level emissions skewness suggests that temporally resolved emission data, regardless of the specific measurement technology, could help operators systematically identify persistently high-emitting facilities and prioritize repairs or operational changes where they will have the greatest impact. Finally, the temporal characteristics of emissions documented here can support reconciliation between bottom-up inventories and top-down observations by providing time-bounded context for large anomalies and by constraining the distribution of emissions below the minimum detection limits of various snapshot measurement technologies.

Several limitations should be considered when interpreting these findings. The analysis is restricted to upstream production facilities equipped with CMS, with a large portion of sites located in the Appalachian and Haynesville basins, which may not be representative of all facilities in these or other basins where infrastructure and practices differ. Furthermore, because the monitored facilities may receive real-time anomaly alerts, event durations and mass contributions reported here may represent a lower bound relative to unmonitored facilities where repairs are not prompted by continuous alerting. CMS-based quantification may also systematically underestimate emission rates during certain high-rate events (highly-pressurized emissions, extremely high rates with plumes whose dynamics are dominated by chemical buoyancy, etc.). More generally, quantification uncertainties, which are currently characterized by controlled release studies, may not capture the full range of operational and environmental conditions encountered in the field. The potential under-detection of very short-lived or poorly advected plumes may further bias some event rates and durations. Finally, the event segmentation framework relies on specific choices for baseline statistics, thresholds, and merging criteria that, while justified for this dataset, may not be optimal in other operational contexts.

Future work should extend this analysis to a broader set of basins and facility types, incorporate operational metadata to distinguish between routine and abnormal emissions, and explore alternative inversion and event-detection schemes. Joint analyses that integrate CMS with other measurement modalities will be particularly valuable for building consistent, multiscale methane inventories that explicitly account for temporal variability and support more effective, measurement-informed mitigation.

Acknowledgements

The authors thank the Environmental Defense Fund for sharing their facility-level emissions distribution data used in this analysis.

References

Bailey, Desmond T (2000). *Meteorological monitoring guidance for regulatory modeling applications*. DIANE Publishing.

Ball, D., U. Ismail, et al. (2025). "Performance Evaluation of Multi-Source Methane Emission Quantification Models Using Fixed-Point Continuous Monitoring Systems". In: *EGUsphere* 2025, pp. 1–50. DOI: 10.5194/egusphere-2025-1266. URL: https://egusphere.copernicus.org/preprints/2025/egusphere-2025-1266/.

Ball, David, Nathan Eichenlaub, and Ali Lashgari (2025). "Performance Evaluation of Fixed-Point Continuous Monitoring Systems: Influence of Averaging Time in Complex Emission Environments". In: *Sensors* 25.9, p. 2801.

Barkley, ZR et al. (2025). "Examining daily temporal characteristics of oil and gas methane emissions in the delaware basin using continuous tower observations". In: *Journal of Geophysical Research: Atmospheres* 130.6, e2024JD042050.

Bell, Clay et al. (2023). "Performance of Continuous Emission Monitoring Solutions under a Single-Blind Controlled Testing Protocol". In: *Environmental Science & Technology* 57.14. PMID: 36977200, pp. 5794–5805. DOI: 10.1021/acs.est.2c09235. eprint: https://doi.org/10.1021/acs.est.2c09235. URL: https://doi.org/10.1021/acs.est.2c09235.

Cheptonui, Fancy et al. (Sept. 2025). "Assessing the performance of emerging and existing continuous monitoring solutions under a single-blind controlled testing protocol". In: *Elementa: Science of the Anthropocene* 13.1, p. 00020. ISSN: 2325-1026. DOI: 10.1525/elementa.2025.00020. eprint: https://online.ucpress.edu/elementa/article-pdf/13/1/00020/899580/elementa.2025.00020.pdf. URL: https://doi.org/10.1525/elementa.2025.00020.

Daniels, William S., Meng Jia, and Dorit M. Hammerling (2024). "Estimating Methane Emission Durations Using Continuous Monitoring Systems". In: *Environmental Science & Technology Letters* 11.11, pp. 1187–1192. DOI: 10.1021/acs.estlett.4c00687. eprint: https://doi.org/10.1021/acs.estlett.4c00687. URL: https://doi.org/10.1021/acs.estlett.4c00687.

Daniels, William S., Douglas W. Nychka, and Dorit M. Hammerling (2025). *A Bayesian hierarchical model for methane emission source apportionment*. arXiv: 2506.03395 [stat.AP]. URL: https://arxiv.org/abs/2506.03395.

Daniels, William S., Jiayang Lyra Wang, et al. (2023). "Toward Multiscale Measurement-Informed Methane Inventories: Reconciling Bottom-Up Site-Level Inventories with Top-Down Measurements Using Continuous Monitoring Systems". In: *Environmental Science & Technology* 57.32. PMID: 37506319, pp. 11823–11833. DOI: 10.1021/acs.est.3c01121. eprint: https://doi.org/10.1021/acs.est.3c01121. URL: https://doi.org/10.1021/acs.est.3c01121.

Hossain, Rafee Iftakhar et al. (Jan. 2026). "A controlled release experiment for investigating methane measurement performance at landfills". In: *Elementa: Science of the Anthropocene* 14.1, p. 00048. ISSN: 2325-1026. DOI: 10.1525/elementa.2025.00048. eprint: https://online.ucpress.edu/elementa/article-pdf/14/1/00048/922142/elementa.2025.00048.pdf. URL: https://doi.org/10.1525/elementa.2025.00048.

Hu, Lei et al. (2025). "An Unexpected Seasonal Cycle in U.S. Oil and Gas Methane Emissions". In: *Environmental Science & Technology* 59.20. PMID: 40366056, pp. 9968–9979. DOI: 10.1021/acs.est.4c14090. eprint: https://doi.org/10.1021/acs.est.4c14090. URL: https://doi.org/10.1021/acs.est.4c14090.

IJzermans, Rutger et al. (2024). "Long-term continuous monitoring of methane emissions at an oil and gas facility using a multi-open-path laser dispersion spectrometer". In: *Scientific Reports* 14.1, p. 623.

Ilonze, Chiemezie et al. (2024). "Assessing the Progress of the Performance of Continuous Monitoring Solutions under a Single-Blind Controlled Testing Protocol". In: *Environmental Science & Technology* 58.25. PMID: 38865299, pp. 10941–10955. DOI: 10.1021/acs.est.3c08511. eprint: https://doi.org/10.1021/acs.est.3c08511. URL: https://doi.org/10.1021/acs.est.3c08511.

Masson-Delmotte, V. et al., eds. (2021). *Climate Change 2021: The Physical Science Basis. Contribution of Working Group I to the Sixth Assessment Report of the Intergovernmental Panel on Climate Change*. Cambridge, UK and New York, NY, USA: Cambridge University Press. DOI: 10.1017/9781009157896.

Omara, Mark et al. (2024). "Constructing a measurement-based spatially explicit inventory of US oil and gas methane emissions (2021)". In: *Earth System Science Data* 16.9, pp. 3973–3991.

Sherwin, Evan et al. (Dec. 2022). "Quantifying oil and natural gas system emissions using one million aerial site measurements". In: DOI: 10.21203/rs.3.rs-2406848/v1.

USEPA (2024). *Estimates of Methane Emissions by Segment in the United States*. Accessed: June 9, 2025. URL: https://www.epa.gov/natural-gas-star-program/estimates-methane-emissions-segment-united-states (visited on 06/09/2025).

– (2025). *Inventory of U.S. Greenhouse Gas Emissions and Sinks: 1990–2022*. Tech. rep. Published April 2024. U.S. Environmental Protection Agency. URL: https://www.epa.gov/ghgemissions/inventory-us-greenhouse-gas-emissions-and-sinks.

Varon, Daniel J. et al. (2026). "Seasonality and Declining Intensity of Methane Emissions from the Permian and Nearby US Oil and Gas Basins". In: *Environmental Science & Technology* 60.1. PMID: 41429418, pp. 425–435. DOI: 10.1021/acs.est.5c08745. eprint: https://doi.org/10.1021/acs.est.5c08745. URL: https://doi.org/10.1021/acs.est.5c08745.

Wang, Jiayang Lyra et al. (2022). "Multiscale Methane Measurements at Oil and Gas Facilities Reveal Necessary Frameworks for Improved Emissions Accounting". In: *Environmental Science & Technology* 56.20. PMID: 36201663, pp. 14743–14752. DOI: 10.1021/acs.est.2c06211. eprint: https://doi.org/10.1021/acs.est.2c06211. URL: https://doi.org/10.1021/acs.est.2c06211.

Williams, James P et al. (2025). "Small emission sources in aggregate disproportionately account for a large majority of total methane emissions from the US oil and gas sector". In: *Atmospheric Chemistry and Physics* 25.3, pp. 1513–1532.